toroidal field below and above r_c varies with the imposed diffusivity contrast $\Delta\eta$. The dashed line is the dependency expected from eq. (248). For relatively low diffusivity contrast, $-1.5 \leq \log(\Delta\eta) \lesssim 0$, both the toroidal field ratio and dynamo period increase as $\sim (\Delta\eta)^{-1/2}$. Below $\log(\Delta\eta) \sim -1.5$, the $\max(B)$-ratio increases more slowly, and the cycle period falls, as can be seen on Fig. 39C. This is basically an electromagnetic skin-depth effect; unlike in the original picture proposed by Parker, here the poloidal field must diffuse down a finite distance into the tachocline before shearing into a toroidal component can commence. With this distance set by our adopted profile of $\Omega(r,\theta)$, as $\Delta\eta$ becomes very small there comes a point where the dynamo period is such that the poloidal field cannot diffuse as deep as the peak in radial shear in the course of a half cycle. The dynamo then runs on a weaker shear, thus yielding a smaller field strength ratio and weaker overall cycle.

{pch_sec:BLsoldyn}

0.27 Babcock-Leighton models

Solar cycle models based on what is now called the Babcock-Leighton mechanism were first developed in the early 1960's, yet they were temporarily eclipsed by the rise of mean-field electrodynamics a few years later. Their revival was motivated in part by the fact that synoptic magnetographic monitoring over solar cycles 21 and 22 has offered strong evidence that the surface polar field reversals are triggered by the decay of active regions (see Fig. 32). The crucial question is whether this is a mere side-effect of dynamo action taking place independently somewhere in the solar interior, or a dominant contribution to the dynamo process itself.

Figure 40 illustrates the basic idea of the Babcock-Leighton mechanism. Consider the bipolar magnetic regions (BMR) sketched on the right. Recall that each of these is the photospheric manifestation of a toroidal flux rope emerging as an Ω-loop (see Fig. 31). The *leading* (*trailing*) component of each BMR is that located ahead (behind) with respect to the direction of the Sun's rotation. Joy's Law states that, on average, the leading component is located at lower latitude than the trailing component, so that a line joining each component of the pair makes an angle with respect to the E-W line. Hale's polarity law also informs us that the leading/trailing magnetic polarity pattern is opposite in each hemisphere, a reflection of the equatorial antisymmetry of the underlying toroidal flux system. Horace W. Babcock (1912–2003) demonstrated empirically from his early magnetographic observation of the sun's surface solar magnetic field that as the BMRs decay (presumably under the influence of turbulent convection), the trailing components drift to higher latitudes, leaving the leading components at lower latitudes, as sketched on Fig. 40 (middle). Babcock also argued that the trailing polarity poloidal flux released to high latitude by the cumulative effects of the emergence and sub-

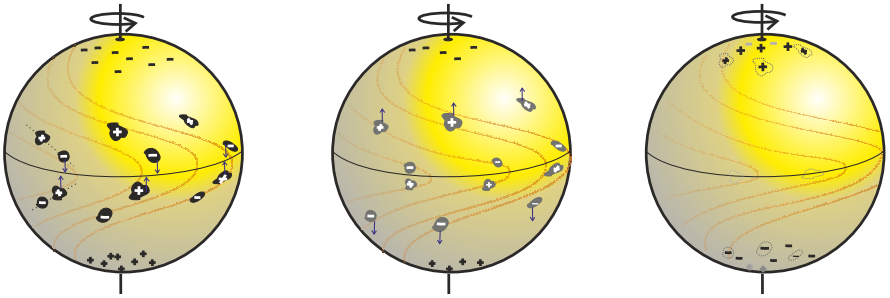

Fig. 40 {F6.1} Cartoon of the Babcock-Leighton mechanism. At left, a number of bipolar magnetic regions (BMR) have emerged, with opposite leading/following polarity patterns in each hemisphere, as per Hale's polarity Law. After some time (middle), the BMRs have started decaying, with the leading components experiencing diffusive cancellation across the equator, while the trailing components have moved to higher latitudes. At later time, (right), the net effect is the buildup of an hemispheric flux of opposite polarity in the N and S hemisphere, i.e., a net dipole moment (see text) Diagram kindly provided by D. Passos.

sequent decay of many BMRs was responsible for the reversal of the sun's large-scale dipolar field (right).

More germane from the dynamo point of view, the Babcock-Leighton mechanism taps into the (formerly) toroidal flux in the BMRs to produce a poloidal magnetic component. To the degree that a positive dipole moment is being produced from a toroidal field that is positive in the N-hemisphere, this is a bit like a positive α-effect in mean-field theory. In both cases the Coriolis force is the agent imparting a twist on a magnetic field; with the α-effect this process occurs on the small spatial scales and operates on individual magnetic fieldlines. In contrast, the Babcock-Leighton mechanism operates on the large scales, the twist being imparted via the the Coriolis force acting on the flow generated along the axis of a buoyantly rising magnetic flux tube.

0.27.1 Sunspot decay and the Babcock-Leighton mechanism {pch_ssec:BLmech}

Evidently this mechanism can operate as sketched on Figure 40 provided the magnetic flux in the leading and trailing components of each (decaying) BMR are separated in latitude faster than they can diffusively cancel with one another. Moreover, the leading components must end up at low enough latitudes for diffusive cancellation to take place across the equator. This is not trivial to achieve, and we now take a more quantitative looks at the Babcock-Leighton mechanism, first with a simple 2D numerical model.

The starting point of the model is the grand sweeping assumption that, once the sunspots making up the bipolar active region lose their cohesiveness, their subsequent evolution can be approximated by the passive advection and resistive decay of the radial magnetic field component. This drastic simplifi-

cation does away with any dynamical effect associated with magnetic tension and pressure within the spots, as well as any anchoring with the underlying toroidal flux system. The model is further simplified by treating the evolution of B_r as a two-dimensional transport problem on a spherical surface corresponding to the solar photosphere. Consequently, no subduction of the radial field can take place.

Even under these simplifying assumptions, the evolution is still governed by the MHD induction equation, specifically its r-component. The imposed flow is made of an axisymmetric surface "meridional circulation", basically a poleward-converging flow in the latitudinal direction on the sphere, and differential rotation in the azimuthal direction:

{E6.10a}
$$\mathbf{u}(\theta) = 2u_0 \sin\theta\cos\theta\hat{\mathbf{e}}_\theta + \Omega_S(\theta) R \sin\theta \hat{\mathbf{e}}_\phi \ , \tag{249}$$

where Ω_S is the solar-like surface differential rotation profile used in the preceding chapter (see eq. (140)). Note that $\nabla\cdot\mathbf{u} \neq 0$, a direct consequence of working on a spherical surface without possibility of subduction. Introducing a new latitudinal variable $\mu = \cos\theta$ and neglecting all radial derivatives, the r-component of the induction equation (evaluated at $r = R$) becomes:

{E6.11}
$$\frac{\partial B_r}{\partial t} = \frac{2u_0}{R}(1-\mu^2)\left[B_r + \mu\frac{\partial B_r}{\partial\mu}\right] - \Omega_S(1-\mu^2)^{1/2}\frac{\partial B_r}{\partial\phi}$$
$$+\frac{\partial}{\partial\mu}\left[\frac{\eta}{R^2}\frac{\partial B_r}{\partial\mu}\right] + \frac{\partial}{\partial\phi}\left[\frac{\eta}{R^2(1-\mu^2)}\frac{\partial B_r}{\partial\phi}\right] \ , \tag{250}$$

with η being the net magnetic diffusivity. As usual, we work with the nondimensional form of eq. (250), now obtained by expressing time in units of $\tau_c = R/u_0$, i.e., the advection time associated with the meridional flow. This leads to the appearance of the following two nondimensional numbers in the scaled version of eq. (250):

{E6.12}
$$\mathrm{R}_m = \frac{u_0 R}{\eta} \ , \qquad \mathrm{R}_u = \frac{u_0}{\Omega_0 R} \ . \tag{251}$$

Using $\Omega_0 = 3\times10^{-6}\,\mathrm{rad\ s^{-1}}$, $u_0 = 15\,\mathrm{m\,s^{-1}}$, and $\eta = 6\times10^8\,\mathrm{m^2 s^{-1}}$ yields $\tau_c \simeq 1.5\,\mathrm{yr}$, $\mathrm{R}_m \simeq 20$ and $\mathrm{R}_u \simeq 10^{-2}$. The former is really a measure of the (turbulent) magnetic diffusivity, and is the only free parameter of the model, as u_0 is well constrained by surface Doppler measurements. The corresponding magnetic diffusion time is $\tau_\eta = R^2/\eta \simeq 26\,\mathrm{yr}$, so that $\tau_c/\tau_\eta \ll 1$.

Figure 41 shows a representative solution. The initial condition (panel A, $t = 0$) describes a series of eight BMRs, four per hemisphere, equally spaced 90^o apart at latitudes $\pm15°$. Each BMR consists of two Gaussian profiles of opposite sign and adding up to zero net flux, with angular separation $d = 10°$ and with a line joining the center of the two Gaussians tilted with respect

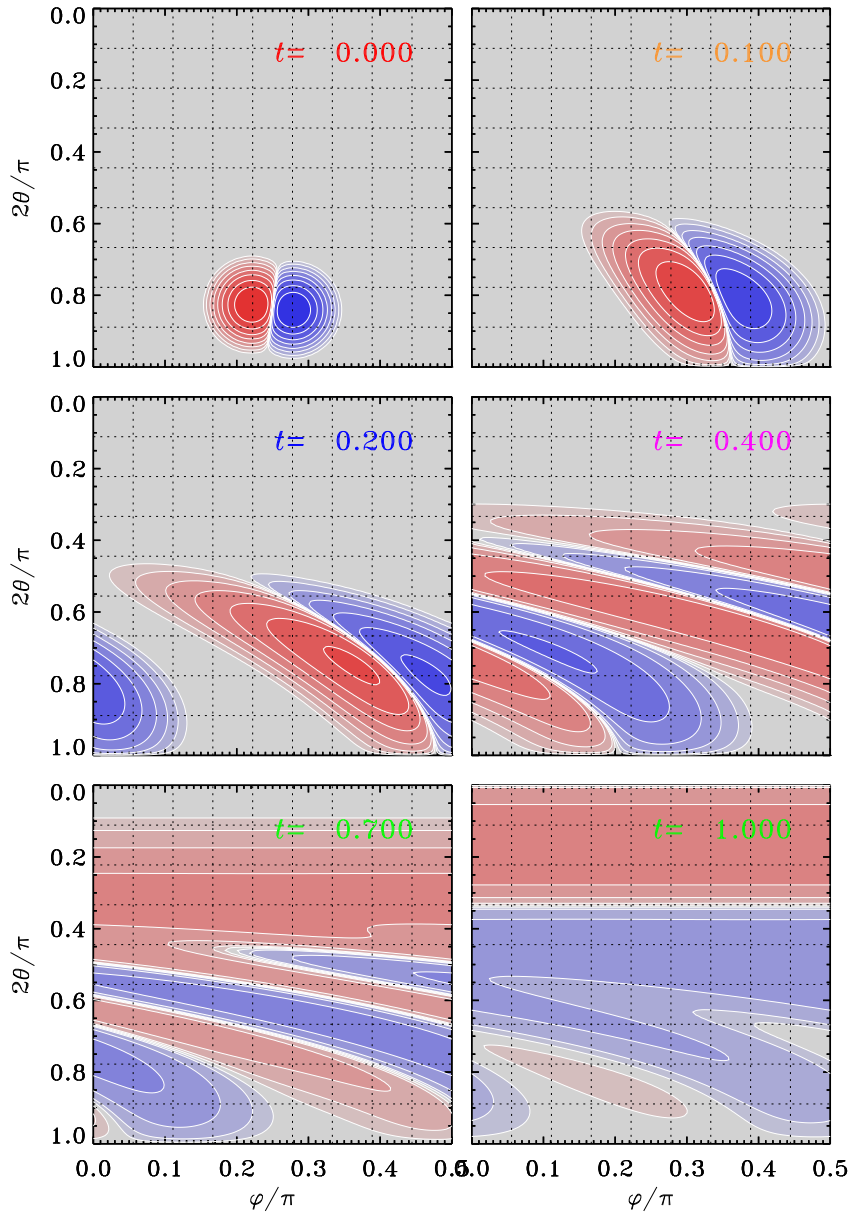

Fig. 41 {F6.2} Evolution of the surface radial magnetic field for two sets of four BMRs equally spaced in longitude, and initially located at latitudes $\pm 15°$, with opposite polarity ordering in each hemisphere, as per Hale's polarity Laws. The surface field evolves in response to diffusion and advective transport by differential rotation and a poleward meridional flow, as described by the 2D advection-diffusion equation (250). Parameter values are $\mathrm{R}_u = 10^{-2}$ and $\mathrm{R}_m = 50$, with time given in units of the meridional flow's characteristic time $\tau_\mathrm{c} = R/u_0$.

to the E-W direction[24] by an angle γ, itself related to the latitude θ_0 of the BMR's midpoint according to the Joy's Law-like relation:

{E6.13}
$$\sin\gamma = 0.5\cos\theta_0 \ . \tag{252}$$

The symmetry of the flow and initial condition on $B_r(\theta,\phi)$ means that the problem can be solved in a single hemisphere with $B_r = 0$ enforced in the equatorial plane, in a 90° wide longitudinal wedge with periodic boundary conditions in ϕ.

The combined effect of circulation, diffusion and differential rotation is to concentrate the magnetic polarity of the trailing "spot" to high latitude, while the polarity of the leading spot dominates at lower latitudes, but experiences diffusive cancellation with the opposite polarity leading flux from it's "cousin" in the other solar hemisphere. At mid-latitudes, the effect of differential rotation is to stretch longitudinally the unipolar regions originally associated with each member of the BMR, causing the development of thin banded structures of opposite magnetic polarities, thus enhancing dissipation.

The combined effects of these advection-diffusion processes is to separate in latitude the two polarities of the BMR. This is readily seen upon calculating the longitudinally averaged latitudinal profiles of B_r, as shown on Fig. 42 for the same six successive epochs corresponding to the snapshots on Fig. 41. The poleward displacement of the trailing polarity "bump" is the equivalent to Babcock's original cartoon (cf. Fig. 40). The time required to achieve this here is $t/\tau_c \sim 1$, and scales as $(R_m/R_u)^{1/3}$. The significant amplification of the trailing polarity bump from $t/\tau_c \gtrsim 0.5$ onward is a direct consequence of magnetic flux conservation in the poleward-converging meridional flow. Notice also the strong latitudinal gradient in B_r at the equator (dotted line) early in the evolution; the associated trans-equatorial diffusive polarity cancellation affects preferentially the leading spots of each pairs, since the trailing spots are located slightly farther away from the equator.

Consider again the mean signed and unsigned magnetic flux:

{E6.13a}
$$\Phi = \mid \langle B_r \rangle \mid \ , \qquad F = \langle \mid B_r \mid \rangle \ , \tag{253}$$

where the averaging operator is now defined on the spherical surface, for the Northern and Southern hemisphere separately:

{E6.13b}
$$\langle B_r \rangle = \int_0^{2\pi} \int_{-\pi/2(0)}^{0(\pi/2)} B_r(\theta,\phi)\sin\theta \mathrm{d}\theta\mathrm{d}\phi \ . \tag{254}$$

Figure 43 shows the time-evolution of the signed (Φ, solid line) and unsigned (F, dashed) fluxes in the Northern hemisphere, for the solution of Fig. 41.

[24] Remember that this is meant to represent the result of a toroidal flux rope erupting through the surface, so that in this case the underlying toroidal field is positive in the Northern hemisphere, which is the polarity of the trailing "spot", as measured with respect to the direction of rotation, from left to right here.

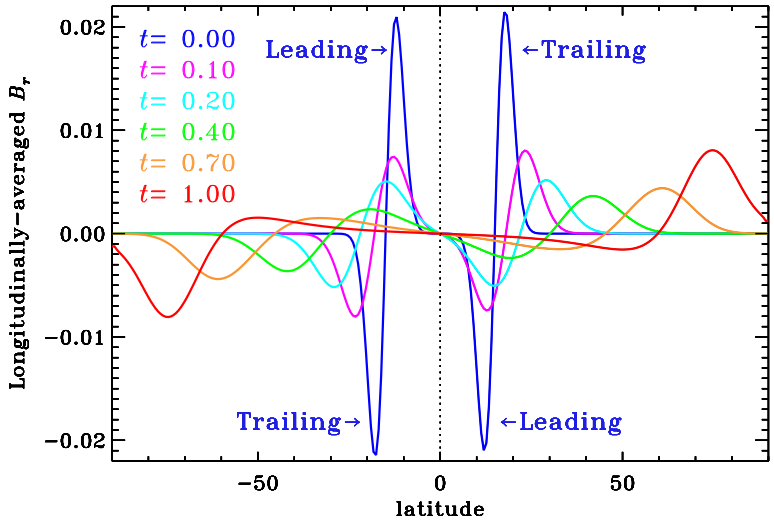

Fig. 42 {F6.2B} Latitudinal profile of the longitudinally averaged vertical magnetic field, at the six epochs plotted on Fig. 41. The strong signal at $t = 0$ results entirely from the slight misalignment of the emerging BMRs with respect to the E-W direction. By one turnover time, two polar caps of oppositely-signed magnetic field have built up, amounting to a net dipole moment (see text).

The unsigned flux decreases rapidly at first, then settles into a slower decay phase. Meanwhile a small but significant hemispheric signed flux is building up. This is a direct consequence of (negative) flux cancellation across the equator, mediated by diffusion, and is the Babcock-Leighton mechanism in action. Note the dual, conflicting role of diffusion here; it is needed for cross-hemispheric flux cancellation, yet must be small enough to allow the survival of a significant trailing polarity flux on timescales of order τ_c.

The efficiency (Ξ) of the Babcock-Leighton mechanism, i.e., converting toroidal to poloidal field, can be defined as the ratio of the signed flux at $t = \tau_c$ to the BMR's initial unsigned flux:

$$\Xi = 2\frac{\Phi(t=\tau_c)}{F(t=0)} \ . \qquad (255) \quad \{\texttt{E6.13c}\}$$

Note that Ξ is independent of the assumed initial field strength of the BMRs since eq. (250) is linear in B_r. Looking back at Fig. 43, one would eyeball the efficiency at about 1% in converting the BMR flux to polar cap signed flux. This conversion efficiency turns out to be a rather complex function of BMR parameters; it is expected to increases with increasing tilt γ, and therefore should increasing with latitudes as per Joy's Law, yet proximity to the equator favors transequatorial diffusive flux cancellation of the leading component;

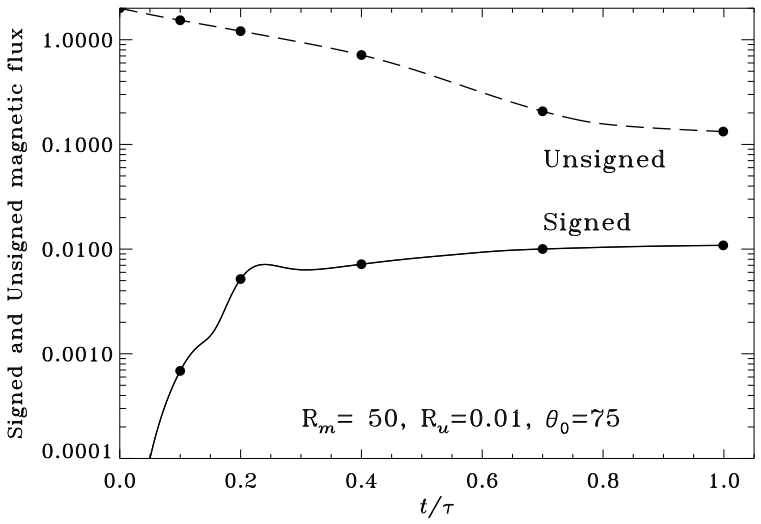

Fig. 43 {F6.3} Evolution of the Northern hemisphere signed (solid line) and unsigned (dashed line) magnetic flux for the solution of Fig. 41. The solid dots mark the times at which the snapshots and longitudinal averages are plotted on Figs. 41 and 42.

moreover, having $\mathrm{d}u_\theta/\mathrm{d}\theta < 0$ favors the separation of the two BMR components, thus minimizing diffusive flux cancellation between the leading and trailing components. These competing effects lead to a toroidal-to-poloidal conversion efficiency peaking for BMRs emerging at fairly low latitudes, the exact value depending on the latitudinal variation of the adopted surface meridional flow profile. At any rate, we noted already (§0.25) that the sun's polar cap flux peaks at solar minimum, at a value amounting to $\sim 0.1\,\%$ of the cycle-integrated active region (unsigned) flux; the efficiency required of the Babcock-Leighton mechanism is indeed quite modest.

0.27.2 Axisymmetrization revisited

Take another look at Fig. 41; at $t = 0$ (panel A) the surface magnetic field distribution is highly non-axisymmetric. By $t/\tau_\mathrm{c} = 0.7$ (panel E), however, the field distribution shows a far less pronounced ϕ-dependency, especially at high latitudes where in fact B_r is nearly axisymmetric. This should remind you of something we encountered earlier: axisymmetrization of a non-axisymmetric magnetic field by an axisymmetric differential rotation (§0.20.5), the spherical analog of flux expulsion. In fact a closer look at the behavior of the unsigned flux on Fig. 43A (dashed line) already shows a hint of the two-timescale be-

havior we have come to expect of axisymmetrization: the rapid destruction of the non-axisymmetric flux component and slower ($\sim \tau_\eta$) diffusive decay of the remaining axisymmetric flux distribution.

Since the spherical harmonics represent a complete and nicely orthonormal functional basis on the sphere, it follows that the initial condition for the simulation of Fig. 41 can be written as

$$B_r^0(\theta,\phi) = \sum_{l=0}^{\infty} \sum_{m=-l}^{+l} b_{lm} Y_{lm}(\theta,\phi) \ , \tag{256}$$ {E6.15}

where the Y_{lm}'s are the spherical harmonics:

$$Y_{lm}(\theta,\phi) = \sqrt{\frac{2l+1}{4\pi}\frac{(l-m)!}{(l+m)!}} P_l^m(\cos\theta) e^{im\phi} \ , \tag{257}$$ {E6.15b}

and with the coefficients b_{lm} given by

$$b_{lm} = \int_0^{2\pi} \int_0^{\pi} B_r^0(r,\theta) Y_{lm}^*(\theta,\phi) \ , \tag{258}$$ {E6.16}

where the "$*$" indicates complex conjugation. Now, axisymmetrization will wipe out all $m \neq 0$ modes, leaving only the $m = 0$ modes to decay away on the slower diffusive timescale[25]. Therefore, at the end of the axisymmetrization process, the radial field distribution now has the form:

$$B_r(\theta) = \sum_{l=0}^{\infty} \sqrt{\frac{2l+1}{4\pi}} b_{l0} P_l^0(\cos\theta) \ , \qquad t/\tau_{\rm c} \gg {\rm R}_u \ . \tag{259}$$ {E6.17}

which now describes an axisymmetric poloidal magnetic field. Voilà!

0.27.3 Dynamo models based on the Babcock-Leighton mechanism

So now we understand how the Babcock-Leighton mechanism can convert a toroidal magnetic field into a poloidal component, and therefore act as a poloidal source term in eq. (172). Now we need to construct a solar cycle model based on this idea. One big difference with the $\alpha\Omega$ models considered in §0.26 is that the two source regions are now spatially segregated: production of the toroidal field takes place in the tachocline, as before, but now production of the poloidal field takes place in the surface layers.

[25] With $\mathbf{u} = 0$, the decay rate of those remaining modes are given by the eigenvalues of the 2D pure resistive decay problem, much like in §0.18.